24th COBEM - 2017

24th ABCM International Congress of Mechanical Engineering
December 3-8, 2017, Curitiba, PR, Brazil

COBEM-2017-0752
EXPERIMENTAL AND NUMERICAL STUDY OF A MICRO HEAT EXCHANGER

Bruna Evelin Gomes
Jacqueline Biancon Copetti
Universidade do Vale do Rio dos Sinos – São Leopoldo, Brazil
bruna.evelin@outlook.com, jcopetti@unisinos.br

Abstract. *In this paper, single-phase liquid flow in microchannels is experimentally and numerically performed. The aluminium micro heat exchanger was developed by machining with 8 parallel channels of 426 μm average hydraulic diameter. An experimental bench was set up for the analysis of the thermal and flow parameters in the exchanger. The temperature distribution in the device, flow regime and local and medium heat transfer coefficient were analysed for different conditions of heat and mass flux. The variation of the mass flux provides lower surface temperatures, the difference between the temperature for the maximum mass flux of 3514 kg/sm² and the minimum of 706 kg/sm² was 30.68ºC. The experimental results were compared with a numerical analysis and differences in temperature up to 7 °C from the numerical over to the experimental were verified. The Reynolds number increases with the heat and the mass flux. The values of average heat transfer coefficient obtained ranged from 5 to 20 kW/m²K for Re from 300 to 1100.*

Keywords: *Micro heat exchanger, single-phase flow in microchannels, heat transfer through microchannels.*

1. INTRODUCTION

The beginning of the use of heat transfer devices occurred in the transport sector: automotive, submarines, aircraft and spacecraft (Kandlikar and Grande, 2002). With the advent of new research on microchannels, its use has to various industrial sectors. Tuckerman and Pease (1981) were the pioneers in the experiments of microchannels for equipment that demanded high performance and high compactness. The heat transfer rates in microchannels are high due to the relation of surface area and volume (Kandlikar, 2010). By reducing the channel diameter, the ratio between the working fluid contact area and the heat sink volume increases, providing an increase in the effective heat exchange area. This increase is accompanied by the increase of the heat transfer coefficient and, consequently, of the heat flow with the reduction of the diameter, further favoring the reduction of the size of the heat exchanger. Heat micro heat exchanger serve applications that have weight and/or volume restrictions (Nascimento and Ribatiski, 2010).

The evolution of the heat transfer devices comes from the following facts, according to Kandlikar et al. (2006),need for greater heat transfer, integrated systems with higher heat generation andnew microscale devices requesting refrigeration. The heat generated by the electronic component is transferred to the cooling liquid by forced convection, the size of the channels causes a reduction in the thickness of the thermal boundary layer, which generates a decrease in the heat transfer resistance by convection, thus generating high rates (Hassan, Phutthavong and Abdelgawad, 2004). Recent researches seek to optimize the geometry of heat exchanger to increase heat transfer with microchannel as Kou et al. (2007) and Sahar et al. (2017). Yang et al. (2017) carried out studies on the geometries of heat exchangers. However, the researches numerically analyzes the heat exchanger with microchannel. There are difficulties in validation of numerically analyzes without the experimental data.

The main objective of this work is to characterize a microchannel heat exchanger with single-phase fluid, presenting the experimentally analyzes and numerically analyzes.

2. EXPERIMENTAL AND COMPUTATIONAL PROCEDURE

2.1 Experimental Model

An experimental bench was built for the tests, with the following equipment:

a) Ultrathermostatic bath with circulation of the manufacturer Quimis to control the temperature of water inlet; b) Interfluid volumetric pump and WEG CW500 frequency inverter for pump control; c) Single-phase voltage variator,

Variac Chuan HSIN for controlling and adjusting the voltage of a thick film resistance of 1kO; d) Omega type E thermocouples; e) Thermal insulation for the elastomeric thermal blanket heat exchanger; f) Agilent 34970A data acquisition system with computer interface for data recording; g) Three-phase power quality analyzer for active, current and voltage measurement model 43B from Fluke manufacturer.

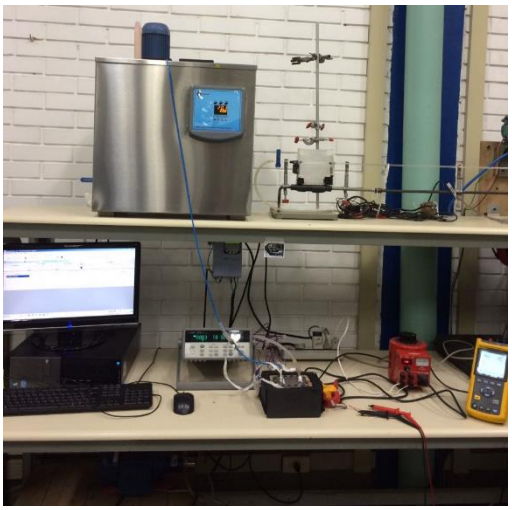

Figure 1. Experimental bench of micro testers heat exchanger

The cooling fluid used is water. The water is cooled to 20 ° C by the bath and circulates in the heat exchanger through the pump, the frequency of which is controlled by the inverter. For each frequency a flow is associated. The heat microtroller is heated by thick film type resistance, the voltage provided by the resistor is controlled by the voltage regulator, the resistance reaches 200 ° C at 220V. Thermal Paste is applied between the heat exchanger contact and the resistance.

Temperature measurements were performed by Type E thermocouples, assembled from 0.30 mm Chromel and Constantan wires and encapsulated in a 1.6 mm stainless steel tube. There are seven thermocouples, two for fluid inlet and outlet temperature measurements, four for wall temperature measurements and one for ambient temperature measurements. The thermocouples used in the experiment were previously calibrated. The outer surface measuring thermocouples of the channels are arranged in the micro heat exchanger along the length of the heat exchanger, the first near the inlet end of the heat exchanger with z = 5 mm and the channel inlet, the next to the center of the exchanger with z = 25 mm, as opposed to that the third thermocouple is measured at the center temperature with z = 30 mm relative to the channel inlet and at the outlet end a thermocouple with z = 45 mm. All thermocouples are 5 mm apart from the surface.

For the tests the laboratory was kept at controlled ambient temperature, between 22 ºC to 24 ºC and the relative humidity in the days of the tests was between 52 to 64%. A total of 24 tests were performed, with heat flows ranging from 8W/cm² to 16.5W/cm² and mass flow from 706 to 3514kg/sm². The piece was heated without water circulation at 80 ° C. With the fluid flowing through the channels, the time of thirty minutes was parameterized for data acquisition. The time was sufficient and the time of thirty minutes was parameterized for the acquisition of data. The time was enough to reach the condition of permanent regime. Control was performed by thermocouple temperature data.

An experimental bench was set up for an analysis of the thermal parameters and the flow in the exchanger. The cooling fluid used is water. The system was instrumented with thermocouples in the inlet and outlet the fluid and in the surface. The temperatures were recorded during the tests for specific conditions of power and flow rate, according to Tab. 1.

Table 1. Operational conditions of tests

Power (W)	30, 42, 53 and 59
Heat Flux, q (W/cm²)	8,12, 15 and 16.5
Volumetric flow rate (ml/min)	33, 42, 55, 93, 116 and 169
Mass flux, G (kg/m²s)	706, 866, 1150, 1939, 2411 and 3514
Initial water temperature (ºC)	20 ºC

The analysis of temperature distribution flow regime and local and medium heat transfer coefficient for different conditions are evaluated.

The figure shows the assembly of the heat exchanger. A 6.60mm² section area o-ring is placed in the channel for the heat exchanger seal. O-ring prevents fluid from flowing out of the heat exchanger. A polycarbonate lid with dimensions of 10x10x1cm is attached to the top of the heat exchanger through bolts and nuts. The plenums of entry and exit are positioned in the respective entrance and exit of the channel. The fluid inlet and outlet is vertical relative to the heat exchanger.

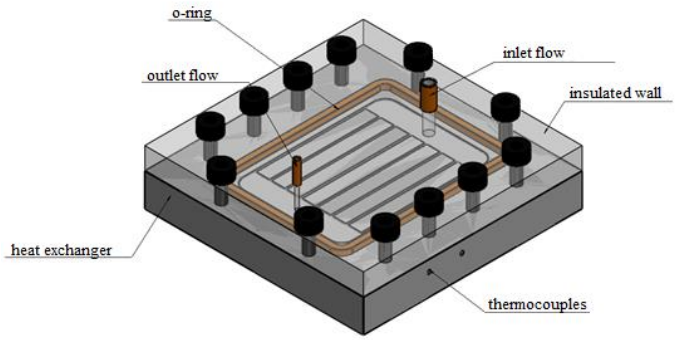

Figure 2. Schematic drawing of test section

The eight rectangular microchannels of the heat exchanger were fabricated on an aluminum substrate with dimensions of 50x50mm. The projected dimensions of the channels are 0.5mm width and 0.2mm height. The inlet and outlet plenum were machined with dimensions of 50x10mm with corners of radius of 4,8mm. An o-ring channel was also machined. The section area of the channel is 6.25mm².

After manufacturing, the channels were measured using the ZEISS® SmartZoom5 microscope and the mean hydraulic diameter is 426 μm (340 μm height x 570 μm width). The magnification obtained with the microscope is 101 times. Images are captured by SmartZeiss ™ software. Eight measurements were taken on different channels. The design of the geometry of the heat exchanger can be seen in the Fig. 3.

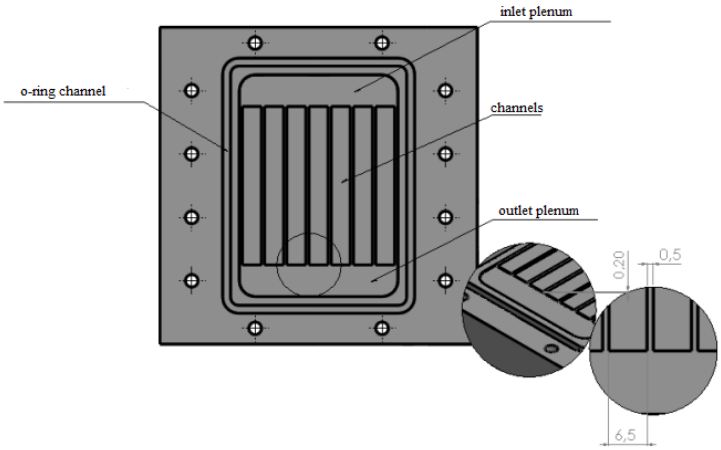

Figure 3. Schematic drawing of heat exchanger machined

2.2 Numerical Analysis

A three-dimensional numerical analysis has been developed and used to compare the experiments data. The simulation has been done using Computational Fluid Dynamics (CFD) software Ansys Fluent 16.1.

In analyzing, the following assumptions were adopted (a) steady state fluid flow and heat transfer, (b) incompressible fluid, (c) fluid is laminar, (d) fluid flow is hydrodynamically fully developed, (e) properties are independent, (f) the system is thermally insulated from the external environment exception surface in contact with the heat source. The residual convergence criterion is 10^{-6}. The hexa and tetrahedron meshing grid scheme was used to the system.

The equations that govern the fluid flow may be expressed as:

Conservation of mass

$$\nabla(\rho \vec{V}) = 0 \tag{1}$$

Conservation of momentum

$$\vec{V}\ \nabla(\rho \vec{V}) = -\nabla P + \nabla(\mu \nabla \vec{V}) \tag{2}$$

Conservation of energy

$$\rho c_p(\vec{V}\ \nabla T) = k\nabla^2 T \tag{3}$$

The equations that govern the solid may be expressed as:

Conservation of mass

$$\nabla(\rho \vec{V}) = 0 \tag{4}$$

Conservation of energy

$$k\nabla^2 T = 0 \tag{5}$$

The governing equations (2), (3) and (5) are solved with a first-order upwind scheme. The simple scheme is used to resolve the solution. The grid convergence index (GCI) was used to valid the numerical analysis. The required error must be less than 5% between maximum temperature. In each mesh the element size was increased by 30% of the previous one. Table 1 shows that the sets of results agree within approximately 0,3462%. Thus, the results were performed by using a mesh of 53008 nodes.

Table 1. Numerical tests for the GCI.

Mesh	Number of nodes	Maximum temperature (°C)
1	15725	63,09
2	26827	56,80
3	53008	56,63

2.3 Data acquisition and processing

Data of ambient temperature, inlet and outlet of the fluid and surface temperatures were recorded every 5 s for each fixed condition of flow and power of Tab.1.

The power applied to the system, or heat removal rate, *qe*, is calculated on the basis as in Eq. (6).

$$q_e = UI \tag{6}$$

Where U is the applied voltage and I is the current.

The heat removal rate can be compared to the rate received by the fluid, qr, through the energy balance as Eq. 7.

$$q_r = \dot{m} cp \Delta T \tag{7}$$

$\dot{m}$ the mass flow rate, cp is the specific heat at the mean temperature and the ΔT is the difference between the outlet and the inlet temperature of the fluid. Based on the inflow rate it is possible to obtain the mass rate as in Eq. (8).

$$\dot{m} = Q\rho \tag{8}$$

Where *Q* is the volume flow ρ rate and density of fluid Equation (9) is heat flux, *q''*.

$$q'' = \frac{q}{A_{sup}} \tag{9}$$

Where A_{sup} é the area of heat sink (Kandlikar et al. 2006) or as Eq. (10).

$$A_{\sup} = (2b\eta f + a)nL \tag{10}$$

Where b is the height of the channel, a is the width of the channel, n the number of channels, L the length of the channel and ηf the fin efficiency. According to Figure 3 a where the length of the fin corresponds to the height of the channel, the thickness of the fin corresponds to the dimension between two channels and the width to the length of the channel. Thus the fin efficiency considering adiabatic end is given by Eq. (11).

$$\eta f = \frac{\tanh(mb)}{mb} \tag{11}$$

The *mb* calculated as Eq. (12).

$$mb = \left(\frac{2h}{ks}\right)b \tag{12}$$

Where h the coefficient of convective heat transfer, k the thermal conductivity of the material and s the spacing between two channels.

In general the works generalize the issue of the flow working with the mass flow, G, given by Eq. (13).

$$G = \frac{\dot{m}/n}{A_{esc}} \tag{13}$$

The mass rate is per channel and the Aesc is the area of the flow section of the channel.

The Reynolds number characterizes the flow regime, Re as in Eq. (14).

$$Re = \frac{GD_h}{\mu} \tag{14}$$

Where the main parameter of the heat exchanger is the hydraulic diameter, Dh, which for rectangular channels is obtained by Eq. (15).

$$Dh = \frac{2ab}{a+b} \tag{15}$$

The local convective heat transfer coefficient, hz, can be determined from the equation of Newton's cooling law for convection or as in Eq. (16):

$$q'' = h_z(T_{sup,z} - T_{f,z}) \tag{16}$$

The temperature of the surface of the exchanger being measured at the position and the temperature of the fluid in the same position, which is calculated from the inlet temperature of the fluid, Te, and the condition of constant heat flux in the wall according to the Eq. (17).

$$T_{f,z} = Te + \frac{q''\,Pz}{\dot{m}cp} \tag{17}$$

Where P is the perimeter of the flow section.

The average coefficient is obtained from the average of the four local coefficients.
The Nusselt number, Nu, can then be obtained by Eq. (18).

$$Nu = \frac{hD_h}{k_f} \tag{18}$$

Where kf is the thermal conductivity of the fluid. Subsequently, this number can be used for comparison with theoretical correlations proposed for Nu and prediction of heat transfer coefficient.

2.4 Results and Discussions

The temperature on the surface of the heat exchanger decreases with increasing liquid flow rate for the same heat flux and inlet temperature, in addition the higher flow rate improves the heat transfer performance. Is possible to see in Figure 4 the distribution of surface temperature along the channel for different mass flux. For the same heat flux (16.5 W/cm²), increasing the mass flux provides lower surface temperatures. Comparing the mass flux of 3514 kg/sm² and 706 kg/sm² at the position of z = 0.045 m, a difference of 30.68 ° C is reached.

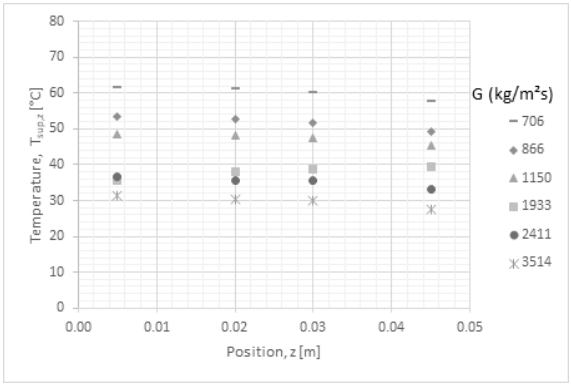

Figure 4. Distribution of wall temperature with the heat flux of 16.5 W/cm² and different mass flux.

Comparing with data from Gudong et al. (2015), the values are good for a power of 48W and a flow of 0.0102m³ / h the maximum temperature reached approximately 46ºC for a heat exchanger of size 4x6mm and hydraulic diameter of 0.1mm.

Figure 5a shows the effect of heat flux on wall temperature distribution along the length of the sink for the lower mass flux. The higher the heat flux, the higher wall temperatures, and the temperature tends to decrease slightly along the length of channels. In Figure 5b the variation of fluid temperature with mass flux for different heat flux is shown. It is found that the temperature difference decreases with increasing mass flux and is higher for higher heat flux.

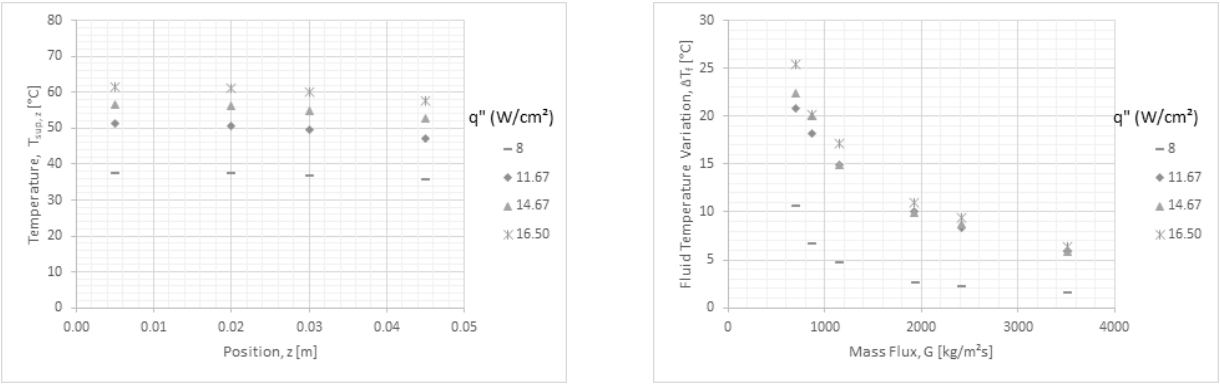

Figure 5. a) Distribution of wall temperature with mass flux of 706 kg/sm² and different heat fluxes; b) Difference of fluid temperature between inlet and outlet.

The increase in heat transfer coefficient with Reynolds number, is shown in Fig. 6. Is possible to see, that the flow regime is laminar and this behavior is similar to that verified by Gunnasegaran (2010), where the increase of the

coefficient of heat transfer with Reynolds was found approximately linear. The increase in the Reynolds number occurs due to the increase of the input velocity in the plenum, which is considered the same velocity in the channels. It is possible to observe in the figure the lower influence of the heat flux. Aliabadi et al. (2016) found values close to 28.5 kW / m²K, with an input power of 50 W, at a mass rate of 0.024 kg / s and channel width of 2 mm.

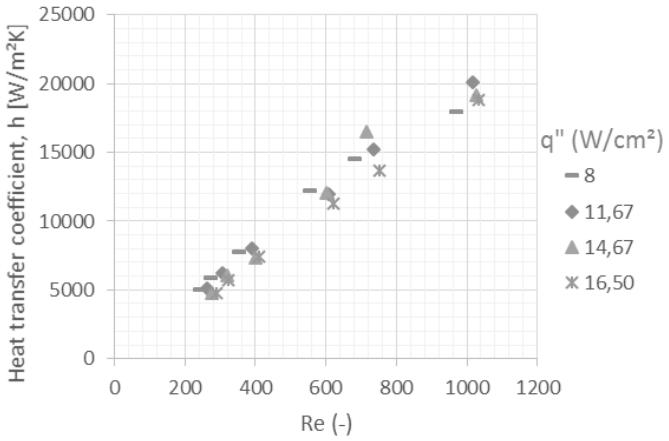

Figure 6. Variation of the heat transfer coefficient with Reynolds number for different heat fluxes.

In the numerical analysis, the case analyzed was for the highest heat flux, that is, 16.5 W/cm² and for the lowest mass flux, 706 kg/sm². The maximum wall temperature is 56.1 °C in outlet plenum. In the same position the fluid temperature is approximately 47.38 °C and in the experimental the value was 49.01 °C.

In Figure 7 it is also possible to check the temperature gradient, similar to that seen in practice.

The local temperature of the surface of the heat exchanger reaching experiment temperatures of higher values. While in the numerical analysis the temperature in the surface was of 38,80 ºC.

However, the numerical analysis showed good qualitative results for checking the fluid temperature gradient and the surface area temperature.

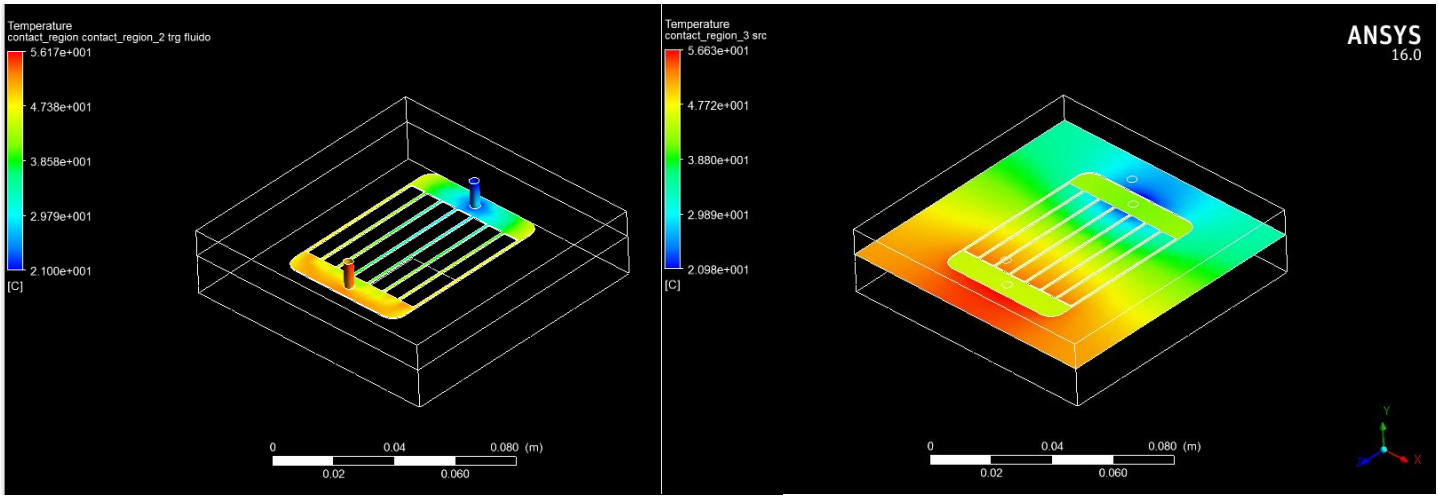

Figure 7. a) Fluid temperature gradient; b) Temperature gradient in the surface area of the heat exchanger.

3. CONCLUSION

Microchannel heat exchanger has good performance for heat transfer at different mass flux and heat flux. The temperature of the wall of the exchanger decreases with the mass flux and depends on the heat flow, increasing the temperature of the liquid, which indicates the good performance of the system for heat dissipation. The lower wall temperatures were reached for the higher mass flux condition. In the operational condition, it criticizes the surface temperature around 60ºC with the highest heat flux and the lowest mass flux. The scheme is laminar according to the Reynolds number agreeing with results of published works in the area. The coefficient of convective heat transfer

obtained reaches values in the range of 5 to 20 kW / m²K. Computational simulation presented good results in relation to the experiment. A difference between a simulation and an experiment varied by 7 ° C for the outlet temperature

4. REFERENCES

Aliabadi, M. Khoshvaght, Et Al., 2016. "*Experimental study on cooling performance of sinusoidal–wavy minichannel heat sink".* Applied Thermal Engineering, n. 92, p.50-61, 2016.

Gundong, Xia et al., 2015. "*Experimental and numerical study of fluid flow and heat transfer characteristics in microchannel heat sink with complex structure"*. Energy Conversion and Management, n 105, p. 848-857, 2015.

Gunnasegaran, P. et al., 2010. "*The effect of geometrical parameters on heat transfer characteristics of microchannels heat sink with different shapes*. International Communications in Heat and Mass Transfer, Vol. 37 (8), p.1078-1086, out. 2010.

Hassan, I.; Phutthavong, P.; Abdelgawad, M., 2004. "Microchannel heat sinks: an overview of the state-of-the-art. Microscale Thermophysical Engineering", v. 8, n. 3, p.183-205, jan. 2004.

Kandlikar, Satish G.; Grande, William J., 2002. "*Evolution of Microchannel Flow Passages – Thermohydraulic Performance and Fabrication Technology*", Proceedings of IMECE 2002 - ASME International Mechanical Engineering Congress & Exposition, New Orleans, p.1-13, nov. 2002.

Kandlikar, Satish G. et al., 2006, "Heat Transfer and Fluid Flow in Minichannels and Microchannels", Elsevier, 2006. 450 p.

Kandlikar, Satish G., 2010. "*History Advances, and Challenges in Liquid Flow and Flow Boiling Heat Transfer in Microchannels: a Critical Review*". Proceedings of the International Heat Transfer Conference, Washington, p.1-20, 13 ago. 2010.

Kou, H-S., Lee, J-J., Chen, C-W., 2007. *"Optimum thermal performance of microchannel heat sink by adjusting channel width and height".* International Communications in Heat and Mass Transfer, n.35, p.577–582, dec. 2016.

Nascimento, Francisco Júlio Do; Ribatski, Gherhardt, 2010. "*Análise da Literatura sobre Dissipadores de Calor Baseados em Multi-microcanais*", VI Congresso Nacional de Engenharia Mecânica, Campina Grande, p. 1-8, 2010.

Sahar, A. M., Wissink, J., Mahmoud, M. M. Karayiannis, T. G. Ishak M. S. A, 2016. *"Effect of hydraulic diameter and aspect ratio on single phase flow and heat transfer in a rectangular microchannel".* Applied Thermal Engineering, n. 155, p. 793-814, may 2016, feb. 2017.

Tuckerman, D. B.; Pease, R. F. W. 1981, "*High-Performance Heat Sinking for VLSI*", IEEE Electron Device Letter, v. 5, n. 2, p.126-129, 1981.

Yang, D., Wang, Y., Ding G., Jin, Z., Zhao, J., Wang, G., 2016. *"Numerical and experimental analysis of cooling performance of single-phase array microchannel heat sinks with different pin-fin configurations".* Applied Thermal Engineering, Vol. 112, p. 1547-1556.

5. RESPONSIBILITY NOTICE

The authors are the only responsible for the printed material included in this paper.